2019 International Conference on Robotics and Automation (ICRA)
Palais des congres de Montreal, Montreal, Canada, May 20-24, 2019

Tetherless Mobile Micro-Surgical Scissors Using Magnetic Actuation

Onaizah Onaizah and Eric Diller

Abstract— **Current minimally-invasive surgical tools suffer from lack of scalability and restricted access to some surgical sites using a laparoscopic probe. This paper introduces a proof-of-concept prototype of the first completely wireless surgical scissors capable of dexterous motion and cutting in a remote environment as a mobile microrobotic device. The 15 mm untethered surgical scissors are custom made from sharpened titanium sheets with a magnet on each blade for actuating force and control. A super-elastic nitinol wire acts as a restoring spring and results in a simple design with no pin joint which is difficult to fabricate at small sizes. To actuate and control the scissors, a 3D magnetic coil system is used here for testing and demonstration. An external magnetic flux density of 20 mT can be generated using the coils and is used for cutting as well as orienting, moving and closing the scissors. In this first prototype setup, the scissors can generate up to 75 mN of cutting force, and we demonstrate the cutting of agar. As a proof of concept demonstration of the potential use of the scissors as a completely untethered surgical tool, we robotically maneuver the scissors to a target location in a confined environment where they cut through agar and return to their initial position.**

I. Introduction

Minimally invasive surgery using laparoscopic and robotic tools has become an increasingly common surgical practice as it minimizes damage to the site, speeds up recovery time and results in fewer complications compared to open surgery [1]. However, challenges to this type of surgery include the use of rigid tools with limited maneuverability, dexterity and minimal degrees of freedom. Robotic tools such as the da Vinci system by Intuitive Surgical [2] allow surgeons to operate away from the tableside using a dexterous controller. Distal tools such as the EndoWrist® instruments by Intuitive Surgical allows for complex tissue manipulation and even suturing by allowing a full rotation of the wrist with tool width as small as 5 mm [1]. These tools are still rigid, unable to maneuver around corners with limited dexterity and therefore have only been adopted in the fields of urology, gynecology, gastroenterology and orthopedics where surgical workspaces are larger and fewer anatomical challenges exist [3].

To access further into the body and overcome some of these limitations, researchers have been developing robotic distal tools which can bend and flex in a tight workspace with a relatively high level of dexterity [4-6]. While these snake-like robots only require one port of entry, one of the biggest limitations of these robots is that due to compliance and motion losses and friction, the position of the end effector cannot always be precisely controlled [7, 8]. The requirement for the use of a single access-point may still necessitate complex surgical planning to reach some sites [9] and severely limits the maneuverability once the tool has navigated to the surgical site.

Completely untethered microrobotic tools have potential to overcome many of these limitations by accessing very small spaces, offering more dexterity [10] and potentially enabling access to areas in the body which are currently inaccessible for minimally invasive procedures. Untethered microrobotic tools have been studied for biopsy and drug delivery applications [11-13] as well as removal of plaque in arteries and blood clots [14], while tissue penetration has been shown with certain tools such as needles [15], and magnetic hammers [16]. However, cutting of soft tissues in a dexterous manner using untethered microrobotic tools such as scissors remains an unexplored problem. The purpose of this work is to test whether a wireless surgical scissors can be developed which can move and cut tissue robotically at a millimeter to centimeter size scale. Leveraging recent advances in microrobotic actuation using magnetic fields [17], we seek to show that adequate cutting force can be achieved and delivered to a simple surgical scissor mechanism which can also be moved in a dexterous manner.

Magnetic actuation is a commonly used remote actuation technique in the field of microrobotics because of its ability to penetrate most environments, generate both force and torque at relatively high speed and because it is safe for use in the human body [10]. Since no on-board power sources are required for magnetic actuation of small tools, scaling down devices even to the single-cell size is possible [18]. Magnetic fields can be generated for dexterous multi-degree-of-freedom manipulation using electromagnets [19] or permanent magnets [20]. Cutting with some untethered magnetically-actuated tools in other applications such as a capsule robot for sampling inside the GI tract [21] and single-cell cutting in an on-chip micro-scale device [22] has been previously demonstrated. However, these designs are not suitable for surgical cutting because they rely on single-use mechanisms or large on-chip actuating magnets and do not generate a scissor motion in a wireless and maneuverable device.

Thus, this study presents the first prototype of an untethered pair of scissors that are magnetically actuated for cutting of soft tissues. The key challenges which must be addressed for the design of viable surgical scissors in a wireless device are a) enforcing a good scissor blade contact and b) achieving a force output large enough to cut tissue. A primary challenge in cutting tissue using a wireless device is in achieving adequate force. The force required for cutting soft tissues varies in the literature and most of these results have been obtained by measuring forces required to penetrate tissue using needles. Tissue penetration forces using needles

We acknowledge the support of the Natural Sciences and Engineering Research Council of Canada (NSERC).

Department of Mechanical and Industrial Engineering, University of Toronto, Toronto, ON M5S 3G9 Canada (e-mail: oonaizah@mie.utoronto.ca, ediller@mie.utoronto.ca)

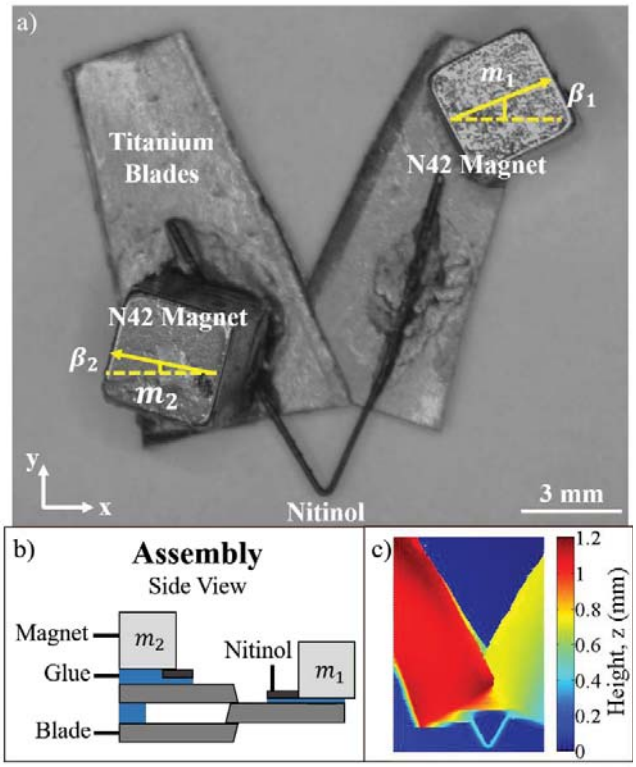

Fig. 1. Scissor design. a) The top view of the scissors showing the layout of blades, magnets and restoring nitinol spring. b) Schematic of scissor design. c) The height of the scissors without the magnets mounted.

have been measured to be 2.5 mN for mouse brain [23] up to 1 N for porcine tissue [24]. Cutting forces using scissors have also been studied for rat and sheep tissues including the liver and were found to be 1.6 N and 7.1 N respectively [25]. It is important to note that these forces varied with the type of scissors and cutting speed used and closing the scissors without cutting required 3.6 N, signifying that these scissors have a very high amount of friction present in the mechanism.

This study outlines the design and fabrication of the prototype scissors and actuating magnetic coil system. As a design tool, a model of scissor cutting is developed and used to optimize the magnetic placement on the scissors. The cutting force is measured, and a demonstration is conducted whereby the scissors are maneuvered from their initial position to a target location where they slice through agarose gel and then return to their initial position.

II. Methods and Materials

A. Design and Fabrication

The proposed prototype design of the scissors features a sandwiched blade structure which minimizes the offset between the blades and keeps them together using a simple design without a pin joint. Cutting with scissors relies on shear forces that arise due to the blades moving on each other. A typical pair of scissors will have a pin joint to keep the blades in close contact. However, on the millimeter scale, this introduces a large amount of friction that tends to jam the actuation. The sandwich blade design naturally keeps the blades together. The blade motion is constrained by a restoring spring which allows the scissors to be closed and opened with a single control input. The scissor design is shown in Fig. 1a. On-board actuation is accomplished by two magnets (with magnetic moment $\boldsymbol{m_1}$ and $\boldsymbol{m_2}$) which are placed at angles (β_1, β_2) as shown in the figure to have a net magnetization direction along the y-axis to orient and move the scissors. Assuming β_1 and β_2 are identical, the net magnetic moment of the entire scissors is

$$m_{net} = m(\sin\beta_1 + \sin\beta_2), \quad (1)$$

where m is the magnitude of the magnetic moment of one magnet. The resulting torque is used align the entire scissors to an externally applied magnetic flux density ($\boldsymbol{B}$) and is given by

$$\boldsymbol{\tau_{net}} = \boldsymbol{m_{net}} \times \boldsymbol{B}, \quad (2)$$

The scissor prototype is custom-made in three manual fabrication steps: 1) grinding, 2) sharpening and 3) assembly. First a thin sheet of titanium (0.1 mm) is cut into a small rectangular strip and then one edge is coarsely ground on a 60-grit wheel. This edge is then sharpened and smoothed on a whetstone with 1000-grit and then 4000-grit. The rectangular strip is then cut into the desired shape as shown in Fig. 1(a) and the scissors are then assembled as shown in Fig. 1b. In this case, a nitinol wire with 193 µm diameter is glued manually using Super Glue. A 3.18 mm cube neodymium iron boron (NdFeB) permanent magnet (grade N42, K&J Magnetics) is mounted on each blade. An angle of 15° for β_1 and β_2 is chosen to provide a net magnetization in the vertical direction to the scissors to allow for movement of the entire scissors device as a mobile microrobotic agent as seen in (1). When an external magnetic field ($\boldsymbol{B}$) is applied, each magnet experiences a magnetic torque which pulls it into alignment with the applied field. These torques close the scissors until the torque is balanced by the nitinol restoring spring. When the magnetic field is removed, the scissors spring back open to their original configuration. All components here were glued together but can also be laser spot welded together.

The height of the top surface of a flipped pair of scissors was measured to ensure that the blades were in sufficiently close contact to allow for cutting. Fig. 1c shows the height (z) of the scissors as measured using a laser scanner (scanCONTROL 2900-10/BL, Micro-Epsilon). The offset between the top blade and the sandwiched blade is approximately 250 µm, which is also the gap between the bottom blade and the sandwiched blade. Since the thickness of the blades is 100 µm, this shows that blades are in close contact.

B. Experimental Setup and Control

A 3-axis electromagnetic coil system is used for all experimental results as shown in Fig. 2. The coils can supply a maximum uniform field of 20 mT in all three directions. The coils are loops of wires arranged in an approximate Helmholtz configuration and each coil is powered by currents supplied by an amplifier (30A8, Advanced Motion Controls), with details given in [13]. If the currents are applied in the same direction, a uniform field can be generated in the center of the workspace. The coils enclose a region of uniform field of approximately 2 cm cube. The scissors are actuated to the target location using open loop control with a game controller. Stick slip motion is used to move the scissors forward on a

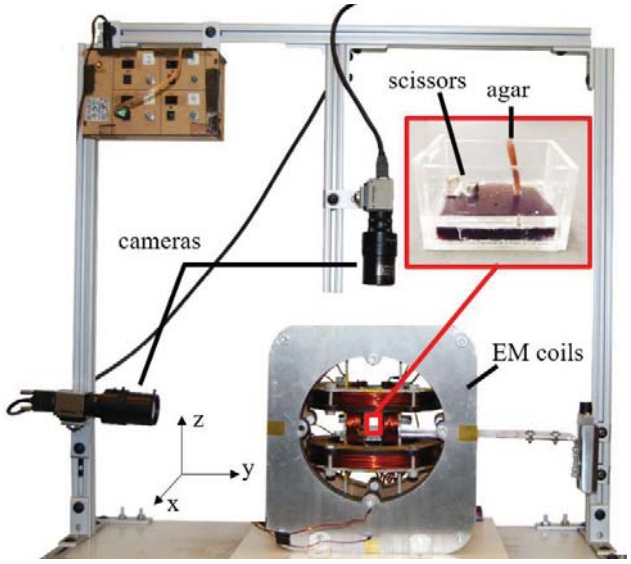

Fig. 2. The actuation setup used for all experiments. A box with the pair of scissors and agar is placed inside the 3 axis Helmholtz coil system and viewed using two cameras (top view and side view).

planar surface, as has been demonstrated in previous works [26]. A 5 mT sawtooth wave with a frequency of 2 Hz is applied in the z-direction with a constant field of 2 mT in the planar direction of motion (x or y). In this way, the scissors rock back and forth, taking a small step (approximately 500 µm each time). The scissors are steered by changing the direction of the horizontal field. Motion of the scissors for cutting, moving and standby modes can be teleoperated or controlled using a high-level feedback controller in future works. Two firewire cameras (FOculus FO124TC) are used for visualization purposes (top view and side view, Fig. 2). The material selected for the cutting demonstration was agarose gel with a concentration of $0.4-0.6\%$ powder because it has been found to have similar mechanical properties to brain tissue [27].

C. Modelling and Design Optimization

To enable optimization of the scissors design, a model of cutting action was developed. One critical design parameter is the placement of the actuating magnets to minimize the effect of inter-magnet forces and torques which can result in poor actuation performance if not controlled. We thus aim to obtain the optimal location for the placement of the magnet ($\boldsymbol{m_2}$) in the region of interest as shown in Fig. 3a. Two repelling dipoles can push the blades far away from each other and require a large magnetic flux density ($\boldsymbol{B}$) to close them fully. Two attracting dipoles can pull the blades closed by overcoming the restoring force of the spring without an external magnetic field being applied leaving no means to open them. Thus, we will seek the placement of magnets which results in zero net interaction (counting the magnetic attraction force and interaction torque) between the two magnets. We will assume $\boldsymbol{m_1}$ is fixed as shown in Fig. 3(a) and vary the position of $\boldsymbol{m_2}$ in this design optimization.

The magnetic dipole interaction force between $\boldsymbol{m_1}$ and $\boldsymbol{m_2}$ is given by

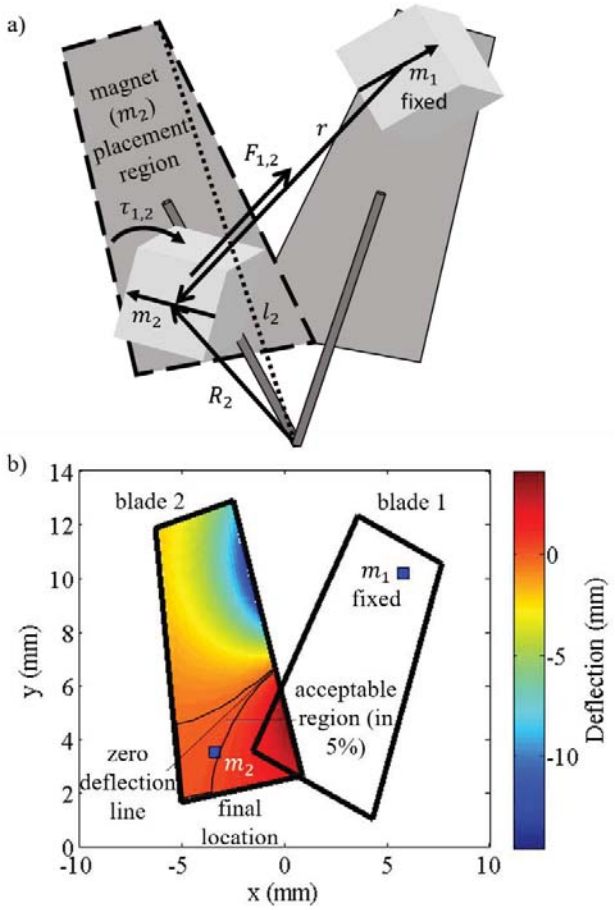

Fig. 3. Scissor magnetic design optimization schematic. a) The top view of the scissors shows the magnetic interaction forces and torques. The placement of the magnet (m_1) is fixed while a region of interest (dashed black line) is shown for the placement of the magnet (m_2). b) The optimal region (< 5% error) for the placement of the magnet (m_2) on the blade is outlined in black. Also, shown in blue is the actual location where it is mounted which falls inside the region and line of zero deflection.

$$\boldsymbol{F_{1,2}} = \frac{3\mu_0}{4\pi r^5}[(\boldsymbol{m_1}\cdot\boldsymbol{r})\boldsymbol{m_2} + (\boldsymbol{m_2}\cdot\boldsymbol{r})\boldsymbol{m_1} + (\boldsymbol{m_1}\cdot\boldsymbol{m_2})\boldsymbol{r} - \frac{5(\boldsymbol{m_1}\cdot\boldsymbol{r})(\boldsymbol{m_2}\cdot\boldsymbol{r})}{r^2}\boldsymbol{r}], \quad (3)$$

where $\boldsymbol{r}$ is the vector from $\boldsymbol{m_1}$ to $\boldsymbol{m_2}$. The resulting torque from this interaction force on the pivot point is shown in (4) and (5) for $\boldsymbol{m_1}$ and $\boldsymbol{m_2}$ respectively where $\boldsymbol{R_1}$ to $\boldsymbol{R_2}$ are the vectors connecting the pivot point to $\boldsymbol{m_1}$ and $\boldsymbol{m_2}$ as

$$\boldsymbol{\tau_{f1}} = \boldsymbol{R_1}\times\boldsymbol{F_{1,2}} \text{ and} \quad (4)$$

$$\boldsymbol{\tau_{f2}} = \boldsymbol{R_2}\times\boldsymbol{F_{1,2}}. \quad (5)$$

The resulting magnetic interaction torque generated by dipole 1 on dipole 2 is given by

$$\boldsymbol{\tau_{1,2}} = \frac{\mu_0}{4\pi r^5}[3\boldsymbol{m_2}\times(\boldsymbol{m_1}\cdot\boldsymbol{r})\boldsymbol{r} - r^2(\boldsymbol{m_2}\times\boldsymbol{m_1})]. \quad (6)$$

There is also a magnetic interaction torque generated by dipole 2 on dipole 1 ($\boldsymbol{\tau_{2,1}}$) which is not shown here for brevity but has an analogous formulation. The magnetic interaction

torque ($\boldsymbol{\tau_{1,2}}$), the resultant torque from the magnetic interaction force ($\boldsymbol{\tau_{f2}}$) and the elastic torque of spring element ($k\boldsymbol{p_{i,2}}$) are in equilibrium as

$$\boldsymbol{\tau_{f2}} + \boldsymbol{\tau_{1,2}} - k\boldsymbol{p_{i,2}} = 0. \quad (7)$$

Here, k is a spring constant that captures the elastic modulus (E), second moment of inertia (I) and length of the spring (L). This calculated deflection is only for the nitinol wire which has a length of 2.6 mm as seen in

$$\boldsymbol{p_{i,2}} = (\boldsymbol{\tau_{f2}} + \boldsymbol{\tau_{1,2}})\frac{L^2}{2EI}. \quad (8)$$

Therefore, this deflection can be extended to the full blade using a similar triangles approach as seen in (9) where l_2 is the length from the pivot to the tip of blade 2. To seek the optimal placement of $\boldsymbol{m_2}$, we consider any point that results in a nominal blade tip deflection below 5% error (or 5% deflection of the total tip to tip separation) as acceptable for the placement of the magnet ($\boldsymbol{m_2}$) as shown in (10). A 5% error translates to a deflection of approximately $\pm$380 µm.

$$\frac{\boldsymbol{p_{f,2}}}{L} = \frac{\boldsymbol{D_2}}{l_2} \quad (9)$$

$$\boldsymbol{D_{i2}} < |0.38| \text{ mm} \quad (10)$$

Fig. 3b shows the region where the magnet $\boldsymbol{m_2}$ can be placed to minimize the magnetic interaction force and torque. While the whole region shown in Fig. 3a or blade was explored, only the small band outlined in Fig. 3b produces a deflection of less than 5% (380 µm) of the tip to tip separation of the blades in the resting position. The line of zero nominal blade tip deflection of the blade is also shown. This is the ideal location for the magnet, but because the magnet is glued manually using tweezers, it cannot be placed accurately on the line. The figure also shows the actual location where the magnet $\boldsymbol{m_2}$ is placed which results in a blade nominal tip deflection of only 290 µm and β_2 of 10°. This is deemed close enough to the optimal location.

Once the location of the second magnet ($\boldsymbol{m_2}$) is finalized, the entire scissors is assembled. We now extend the model to include the actuating torque ($\boldsymbol{\tau_{m2}}$) due to an externally applied magnetic flux density ($\boldsymbol{B}$) during actuation as given by

$$\boldsymbol{\tau_{m2}} = \boldsymbol{m_2} \times \boldsymbol{B}. \quad (11)$$

Again, the equation is only shown for $\boldsymbol{m_2}$, but an analogous formulation exists for the magnet $\boldsymbol{m_1}$ which is used to calculate the deflection of blade 1. The deflection of each blade $\boldsymbol{p_{f,1}}$ and $\boldsymbol{p_{f,2}}$ is calculated as

$$\boldsymbol{p_{f,1}} = (\boldsymbol{\tau_{f1}} + \boldsymbol{\tau_{2,1}} + \boldsymbol{\tau_{m1}})\frac{L^2}{2EI} \text{ and} \quad (12)$$

$$\boldsymbol{p_{f,2}} = (\boldsymbol{\tau_{f2}} + \boldsymbol{\tau_{1,2}} + \boldsymbol{\tau_{m2}})\frac{L^2}{2EI}. \quad (13)$$

Similar to the previous section, this calculated deflection is only for the nitinol wire which has a length of 2.6 mm. Therefore, this deflection is similarly extended to the full blade using a similar triangles approach as seen in (9) where l_1 and l_2 are the distances from the pivot point to the tip of blade 1 and blade 2 respectively. The model iteratively updates the position of the magnets $\boldsymbol{m_1}$ and $\boldsymbol{m_2}$ based on the previous deflection of the blades. This updated position is used to calculate updated torques until a converged solution is reached. The resulting deflections $\boldsymbol{D_{f1}}$ (for blade 1) and $\boldsymbol{D_{f2}}$ are subtracted from the initial position of the blade separation to obtain the tip to tip separation ($\boldsymbol{d}$) of the blades from 0 – 14 mT as shown in Fig. 4a and (14).

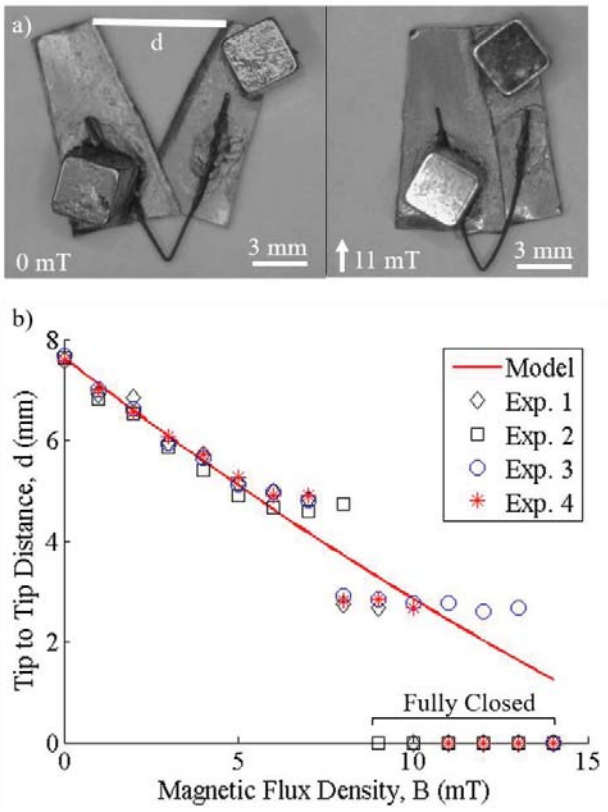

Fig. 4. a) The tip to tip distance (d) between the blades is shown at 0 mT and 11 mT. b) The measured and modelled tip to tip distance as a function of magnetic flux density (B) for a set of unloaded scissors is plotted.

$$\boldsymbol{d}(\boldsymbol{B}) = d(0) - \boldsymbol{D_1} - \boldsymbol{D_2} \quad (14)$$

III. Results

A. Model Validation

The tip to tip separation of the blades ($\boldsymbol{d}$) under varying applied field is plotted in Fig. 4b. The experimental data is based on 4 experimental measurements taken at different field strengths, while the model is from (14). A large deviation is seen for the last few data points ranging from 9 mT to 14 mT, which we attribute to two primary reasons. The first and most apparent one is that there is friction present in the scissors that is not captured by the model. The second reason is that it is possible that the nitinol enters a nonlinear deformation regime at high strains.

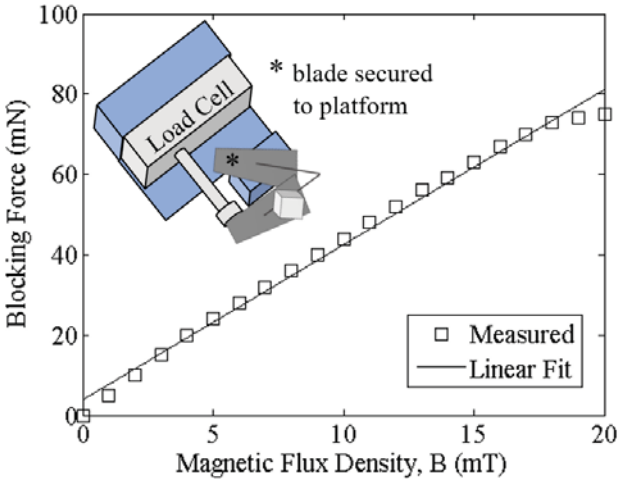

Fig. 5. The blocking force of the scissors is measured to get an estimate of the force required for cutting agar using the image shown in the inset. This setup is placed inside the 3-axis coils.

B. Force Measurements

The blocking force of the scissors was measured using a single-axis 100 g load cell (GSO100, Transducer Technologies), which has a rated accuracy of ± 0.8 mN. The measurement is shown in Fig. 5. In this measurement, one blade of the scissors is pushed into contact with the load cell measuring rod but does not move during the measurement. The other blade of the scissors is glued to the platform and not able to move. One important thing to note here is that the magnet $\boldsymbol{m_1}$ has been removed from the scissors for the purposes of this experiment. This is to remove any magnetic interaction with the load cell, but it is possible that this removal may have a small impact on the force output. However, the scissors were optimized to minimize the magnetic interaction forces and torques while in resting position, so we expect this error to be small.

The resultant forces vs. magnetic flux density are plotted in Fig. 5. A maximum force of 75 mN is achieved at an applied flux density of 20 mT, which is the largest magnetic flux density output by the coils. If the scissors fully close at 9 mT, 35 mN can be used for cutting. However, if the scissors close at 14 mT, only 16 mN of the force is used for cutting. Since it is not possible to separate the closing and cutting motions of the scissors, we can conclude that the cutting force falls between the 16 mN to 35 mN range.

C. Robotic Motion and Cutting Demonstration

A demonstration of cutting agarose gel is shown in the supplementary video. The scissors are placed inside a 32 x 29 x 21 mm box along with a small strip of agar dyed red. The bottom of the box is also lined with agar dyed red. An acrylic plate with a hole is placed on top of this lining. The agar strip is fed up from the hole to ensure that it stays vertical. The box is filled with 1 cSt silicone oil and all experiments are performed in this liquid.

The scissors are maneuvered from their initial position using stick slip motion to the target location where an agar tower is sliced using a field strength of 20 mT. The scissors are then maneuvered back to their initial position. Five screenshots from the video are shown in Fig. 6 where the scissors are shown: i) at their initial position, ii) before cutting, iii) during cutting, iv) immediately after cutting, v) home position.

IV. Conclusions

The pair of scissors proposed in this study are 15 mm x 15 mm when fully open and 11 mm wide when fully closed. This is approximately two times the desired size for clinical use. Typically, neurosurgeons use small surgical corridors via burr holes through which instruments are fed through and the scissors would have to fit through this corridor. The scissors can easily be scaled down and a larger external magnetic flux density can be used to generate the same force output.

The rat liver required approximately 1.6 N to cut with a pair of scissors and sheep liver approximately 7.1 N [25]. The cutting force achieved here is between 16-35 mN and would need to be increased to cut these tissues. This can be done by using larger external magnetic flux densities. Recent advances in clinical-scale coil systems have shown capabilities to produce fields up to 400 mT [19] which is 20

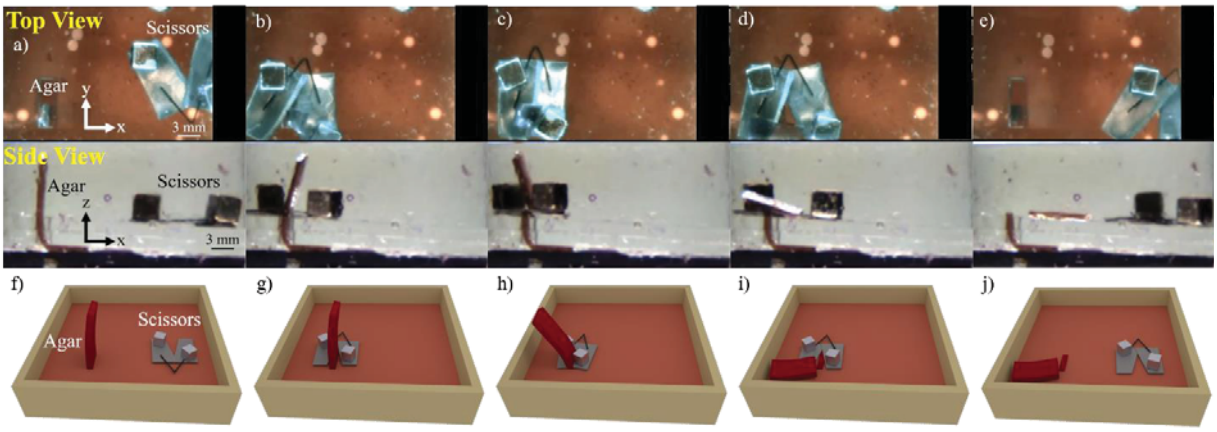

Fig. 6. a)-e) The scissors are shown moving from their initial position to the agar and cutting it and then moving back. Both the top and side camera views are shown. f)-j) A simulation of the scissors moving from their initial location to the agar and cutting it and then moving back is shown. The simulation matches the snapshots of the video.

times larger than the maximum field strength used in this study. Using such a large field, the force output of the scissors would be increased to 1.5 N which is close to the value required for rat liver. In future work we will investigate cutting forces at higher field strength, which would also allow for the reduction of the size of the surgical scissors here. Further work is needed to achieve smooth cutting motion for dexterous procedures as friction effects are seen here which cause the scissors to stick during the closing and can reduce the cutting force produced. The scissors motion and cutting demonstration here was a relatively simple motion in a 2D plane. Future work will develop a robust 3D controller for accurate feedback-controlled positioning and cutting in arbitrary environments. Future studies will explore the cutting of real tissue, explore smaller scissors, control the 3D positioning and the use of medical imaging as real-time feedback to further prove the potential of using untethered surgical tools. The safety and usability of completely untethered tools is a potential concern depending on the application scenario. One way this concern could be addressed is by adding an extremely flexible cable to the scissors for scissor removal.

V. Acknowledgements

The authors acknowledge Tianqi Xu for technical support.

VI. References

[1] N. Simaan, R. M. Yasin, and L. Wang, "Medical Technologies and Challenges of Robot-Assisted Minimally Invasive Intervention and Diagnostics," *Annual Review of Control, Robotics, and Autonomous Systems,* vol. 1, no. 1, pp. 465-490, 2018.

[2] I. A. M. J. Broeders and J. Ruurda, "Robotics revolutionizing surgery: the Intuitive Surgical "Da Vinci" system," *Industrial Robot: An International Journal,* vol. 28, no. 5, pp. 387-392, 2001.

[3] J. J. Doulgeris, S. A. Gonzalez-Blohm, A. K. Filis, T. M. Shea, K. Aghayev, and F. D. Vrionis, "Robotics in Neurosurgery: Evolution, Current Challenges, and Compromises," *Cancer Control,* vol. 22, no. 3, pp. 352-359, 2015.

[4] T. Ota, A. Degani, D. Schwartzman, B. Zubiate, J. McGarvey, H. Choset*, et al.*, "A Highly Articulated Robotic Surgical System for Minimally Invasive Surgery," *The Annals of thoracic surgery,* vol. 87, no. 4, pp. 1253-1256, 2009.

[5] J. Burgner-Kahrs, D. C. Rucker, and H. Choset, "Continuum Robots for Medical Applications: A Survey," *IEEE Transactions on Robotics,* vol. 31, no. 6, pp. 1261-1280, 2015.

[6] C. Bergeles, A. H. Gosline, N. V. Vasilyev, P. J. Codd, P. J. d. Nido, and P. E. Dupont, "Concentric Tube Robot Design and Optimization Based on Task and Anatomical Constraints," *IEEE Transactions on Robotics,* vol. 31, no. 1, pp. 67-84, 2015.

[7] V. Agrawal, W. J. Peine, B. Yao, and S. Choi, "Control of cable actuated devices using smooth backlash inverse," in *IEEE International Conference on Robotics and Automation*, 2010, pp. 1074-1079.

[8] N. Simaan, X. Kai, W. Wei, A. Kapoor, P. Kazanzides, R. Taylor*, et al.*, "Design and Integration of a Telerobotic System for Minimally Invasive Surgery of the Throat," *The International Journal of Robotics Research,* vol. 28, no. 9, pp. 1134-1153, 2009.

[9] L. G. Torres, C. Baykal, and R. Alterovitz, "Interactive-rate motion planning for concentric tube robots," in *2014 IEEE International Conference on Robotics and Automation (ICRA)*, 2014, pp. 1915-1921.

[10] M. Sitti, H. Ceylan, W. Hu, J. Giltinan, M. Turan, S. Yim*, et al.*, "Biomedical Applications of Untethered Mobile Milli/Microrobots," *Proceedings of the IEEE,* vol. 103, no. 2, pp. 205-224, 2015.

[11] E. Gultepe, J. S. Randhawa, S. Kadam, S. Yamanaka, F. M. Selaru, E. J. Shin*, et al.*, "Biopsy with Thermally-Responsive Untethered Microtools," *Advanced Materials,* vol. 25, no. 4, pp. 514-519, 2012.

[12] E. Diller and M. Sitti, "Three-Dimensional Programmable Assembly by Untethered Magnetic Robotic Micro-Grippers," *Advanced Functional Materials,* vol. 24, no. 28, pp. 4397-4404, 2014.

[13] J. Zhang, O. Onaizah, K. Middleton, L. You, and E. Diller, "Reliable Grasping of Three-Dimensional Untethered Mobile Magnetic Microgripper for Autonomous Pick-and-Place," *IEEE Robotics and Automation Letters,* vol. 2, no. 2, pp. 835-840, 2017.

[14] I. S. M. Khalil, D. Mahdy, A. E. Sharkawy, R. R. Moustafa, A. F. Tabak, M. E. Mitwally*, et al.*, "Mechanical Rubbing of Blood Clots Using Helical Robots Under Ultrasound Guidance," *IEEE Robotics and Automation Letters,* vol. 3, no. 2, pp. 1112-1119, 2018.

[15] A. C. Barnett, J. A. Jones, Y.-S. Lee, and J. Z. Moore, "Compliant Needle Vibration Cutting of Soft Tissue," *Journal of Manufacturing Science and Engineering,* vol. 138, no. 11, p. 111011, 2016.

[16] J. Leclerc, A. Ramakrishnan, N. V. Tsekos, and A. T. Becker, "Magnetic Hammer Actuation for Tissue Penetration Using a Millirobot," *IEEE Robotics and Automation Letters,* vol. 3, no. 1, pp. 403-410, 2018.

[17] M. P. Kummer, J. J. Abbott, B. E. Kratochvil, R. Borer, A. Sengul, and B. J. Nelson, "OctoMag: An Electromagnetic System for 5-DOF Wireless Micromanipulation," *IEEE Transactions on Robotics,* vol. 26, no. 6, pp. 1006-1017, 2010.

[18] B. J. Nelson, I. K. Kaliakatsos, and J. J. Abbott, "Microrobots for Minimally Invasive Medicine," *Annual Review of Biomedical Engineering,* vol. 12, no. 1, pp. 55-85, 2010.

[19] J. Rahmer, C. Stehning, and B. Gleich, "Remote magnetic actuation using a clinical scale system," *PLOS ONE,* vol. 13, no. 3, p. e0193546, 2018.

[20] P. Ryan and E. Diller, "Magnetic Actuation for Full Dexterity Microrobotic Control Using Rotating Permanent Magnets," *IEEE Transactions on Robotics,* vol. 33, no. 6, pp. 1398-1409, 2017.

[21] M. Simi, G. Gerboni, A. Menciassi, and P. Valdastri, "Magnetic Torsion Spring Mechanism for a Wireless Biopsy Capsule," *Journal of Medical Devices,* vol. 7, no. 4, p. 041009, 2013.

[22] M. Hagiwara, T. Kawahara, Y. Yamanishi, and F. Arai, "Precise Control of Magnetically Driven Microtools for Enucleation of Oocytes in a Microfluidic Chip," *Advanced Robotics,* vol. 25, no. 8, pp. 991-1005, 2011.

[23] A. A. Sharp, A. M. Ortega, D. Restrepo, D. Curran-Everett, and K. Gall, "In Vivo Penetration Mechanics and Mechanical Properties of Mouse Brain Tissue at Micrometer Scales," *IEEE transactions on bio-medical engineering,* vol. 56, no. 1, pp. 45-53, 2009.

[24] M. Khadem, C. Rossa, R. S. Sloboda, N. Usmani, and M. Tavakoli, "Mechanics of Tissue Cutting During Needle Insertion in Biological Tissue," *IEEE Robotics and Automation Letters,* vol. 1, no. 2, pp. 800-807, 2016.

[25] S. Greenish, V. Hayward, V. Chial, A. Okamura, and T. Steffen, "Measurement, Analysis, and Display of Haptic Signals During Surgical Cutting," *Presence: Teleoperators and Virtual Environments,* vol. 11, no. 6, pp. 626-651, 2002.

[26] C. Pawashe, S. Floyd, and M. Sitti, "Dynamic Modeling of Stick Slip Motion in an Untethered Magnetic Micro-Robot," in *Robotics: Science and Systems*, 2008.

[27] F. Pervin and W. W. Chen, "Mechanically Similar Gel Simulants for Brain Tissues," in *Dynamic Behavior of Materials, Volume 1*, 2011, pp. 9-13.